# Supplementary information

# Earthworm Inspired Lubricant Self-Pumping Hydrogel with Sustained Lubricity at High Loading

Shuanhong Ma[1,2 #], Lunkun Liu[1,3 #], Weiyi Zhao[1], Renjie Li[1], Xiaoduo Zhao[1,2], Yunlei Zhang[1], Bo Yu[1], Ying Liu[3] *, Feng Zhou[1] *

**1** State Key Laboratory of Solid Lubrication, Lanzhou Institute of Chemical Physics, Chinese Academy of Sciences, Lanzhou, 730000, China

**2** Shandong Laboratory of Advanced Materials and Green Manufacture at Yantai, Yantai Zhongke Research Institute of Advanced Materials and Green Chemical Engineering, Yantai, 264006, China

**3** School of Advanced Manufacturing, Nanchang University, Nanchang, 330031, China

*Correspondence authors email:
lying@ncu.edu.cn (Y.L.); zhouf@licp.cas.cn (F.Z.)

*# Shuanhong Ma and Lunkun Liu contribute equal to this work.*

**This PDF file includes:**

Supplementary Figs. 1 to 32

**Other Supplementary Materials for this manuscript include the following:**

Supplementary Movies 1 to 4

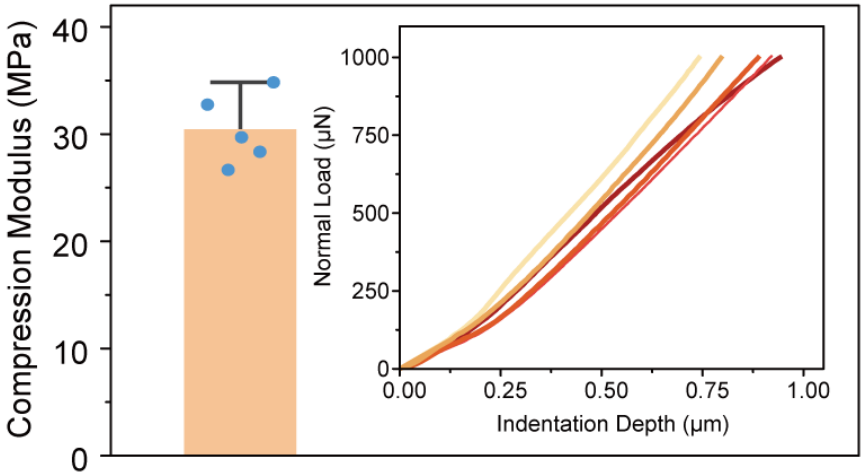


**Supplementary Fig. 1 | Mechanical property of hydrogel matrix.** Compression elastic modulus of the mechanically robust double-crosslinked hydrogel matrix ((P(AAm-AA)/Fe)) used for generation of dissociation lubrication layer. (n=5, mean± SD)

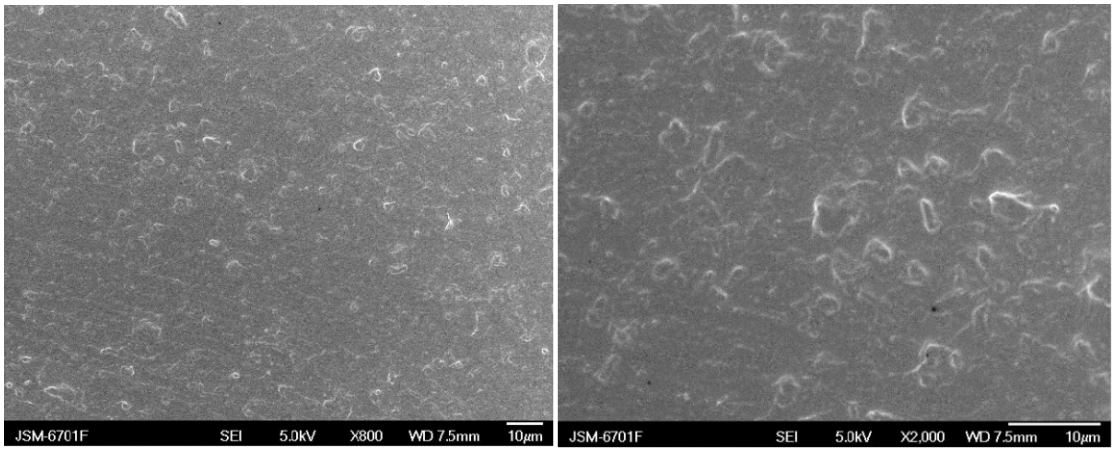


**Supplementary Fig. 2 | Micro-structure characterization of hydrogel matrix.** Surface morphology of double-crosslinked hydrogel matrix ((P(AAm-AA)/Fe)) captured by FE-SEM (the sample was treated by *in situ* freezing-drying).

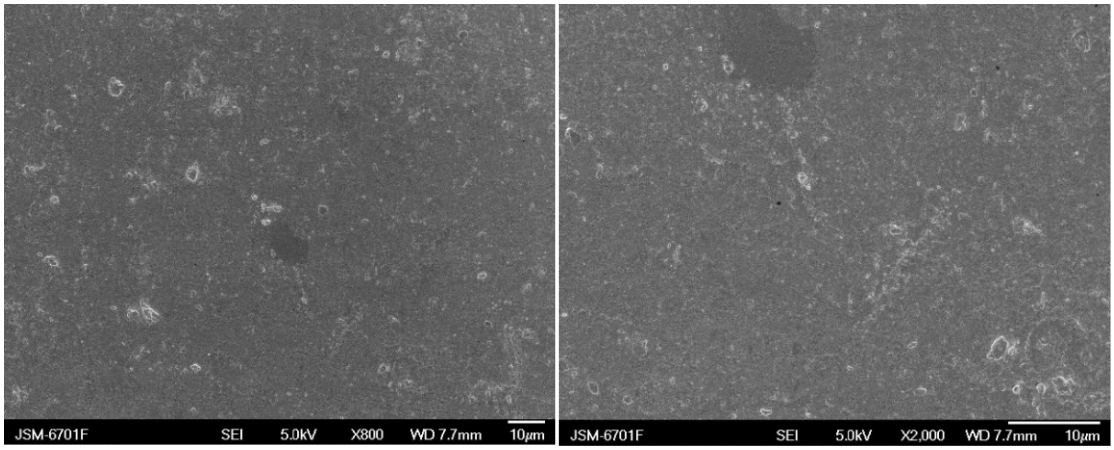


**Supplementary Fig. 3 | Micro-structure characterization of hydrogel matrix.** Cross-section morphology of double-crosslinked hydrogel matrix ((P(AAm-AA)/Fe)) captured by FE-SEM (the sample was treated by *in situ* freezing-drying).

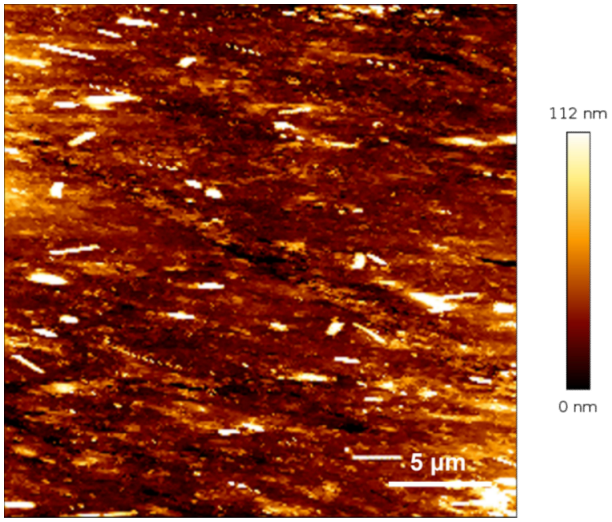


**Supplementary Fig. 4 | Network structure characterization of hydrogel matrix.** Surface micro-morphology of double-crosslinked hydrogel matrix ((P(AAm-AA)/Fe)) captured by AFM.

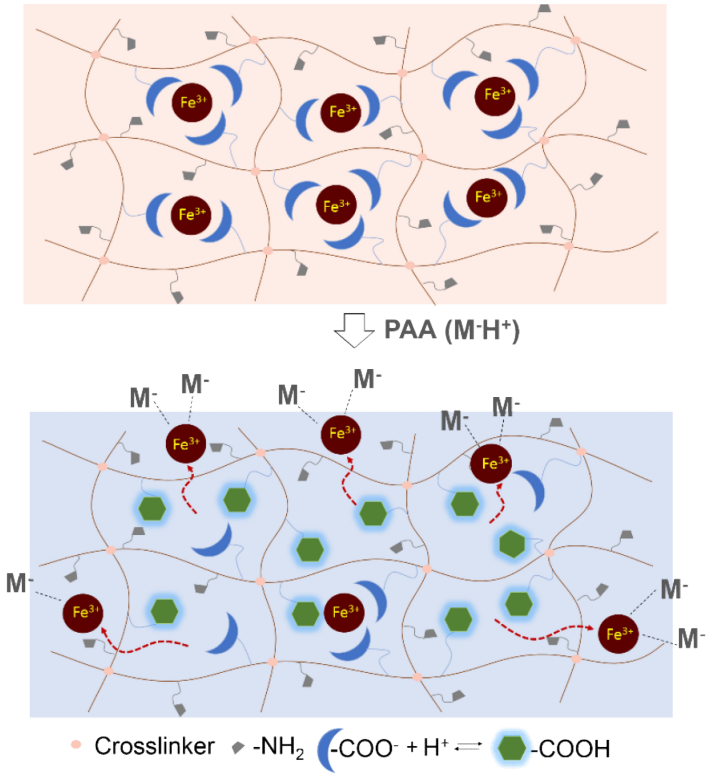


**Supplementary Fig. 5 | Dissociation mechanism for generating lubrication layer.** The mechanism for generating dissociation lubrication layer on surface of mechanically robust double-crosslinked hydrogel matrix.

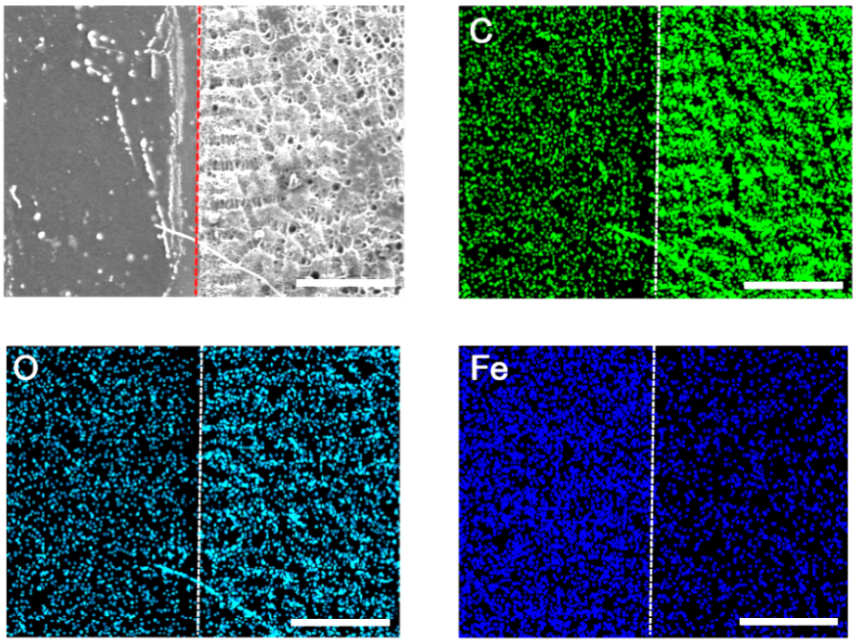


**Supplementary Fig. 6 | Components analysis of SLH.** Surface EDS mapping results (C, O, Fe) for dissociation lubrication layer (the mechanically robust double-crosslinked hydrogel matrix is used as comparison). Scale bar: 10 μm.

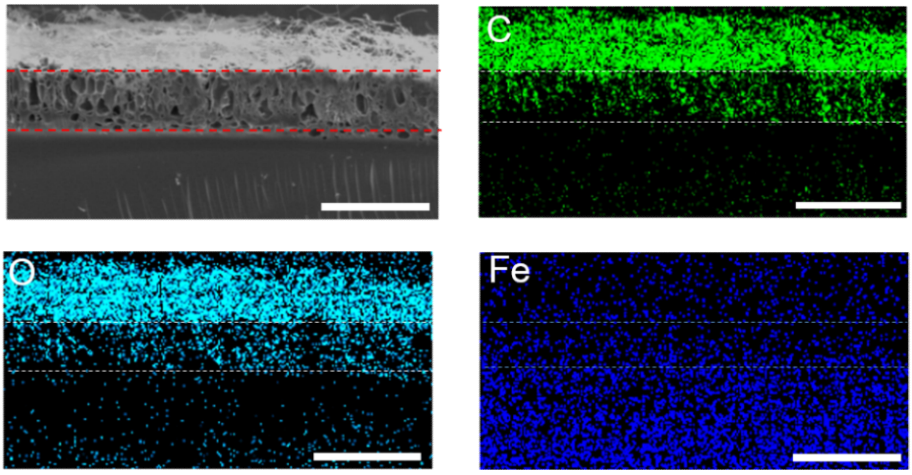


**Supplementary Fig. 7 | Components analysis of SLH.** Cross-sectional EDS mapping results (C, O, Fe) for dissociation lubrication layer and the mechanically robust double-crosslinked hydrogel matrix. Scale bar: 200 μm.

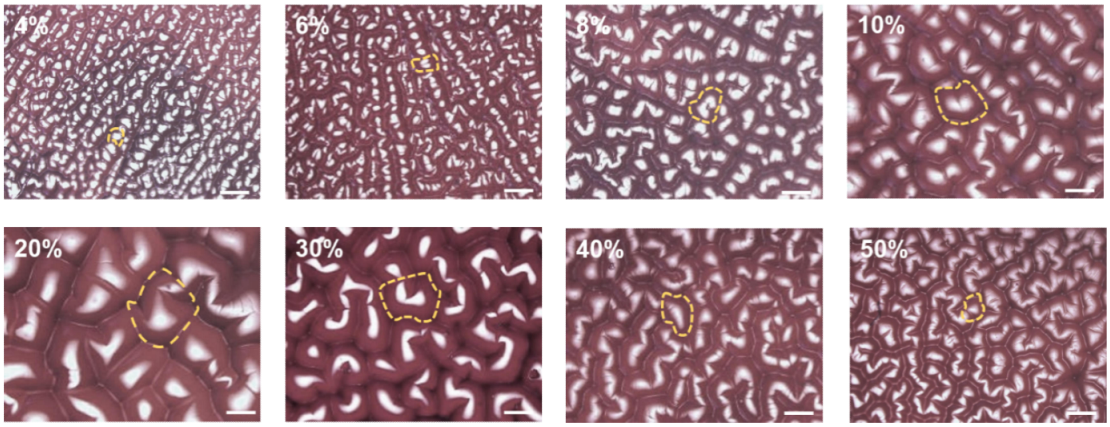


**Supplementary Fig. 8 | Concentrations-dominated surface morphology of dissociation layer.** Periodic but non-regular surface wrinkles morphologies of SLH samples obtained by controllable dissociation with different PAA mass concentrations (dissociation time: 8 h) to generate soft lubrication layer. Scale bar: 100 μm.

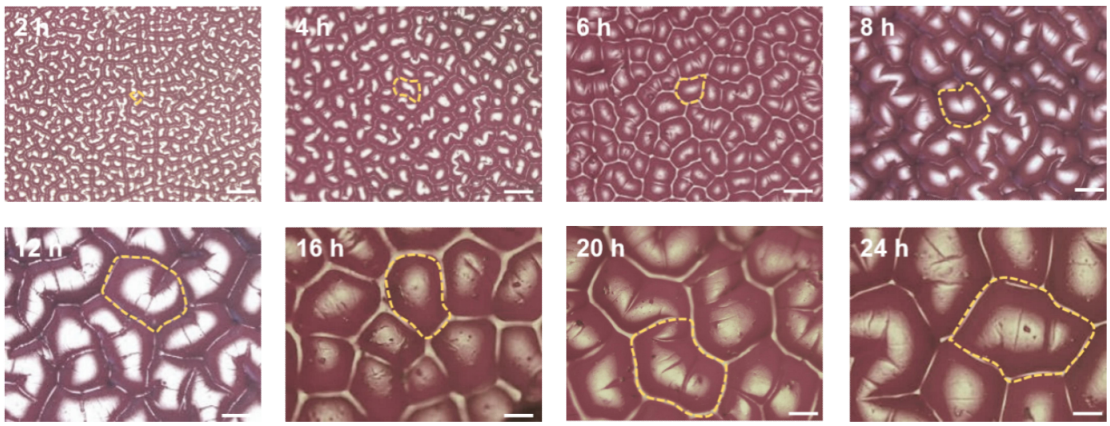


**Supplementary Fig. 9 | Time-dominated surface morphology of dissociation layer.** Periodic but non-regular surface wrinkles morphologies of SLH samples obtained by controllable PAA dissociation with different immersing time (mass concentration: 10%) to generate soft lubrication layer. Scale bar: 100 μm.

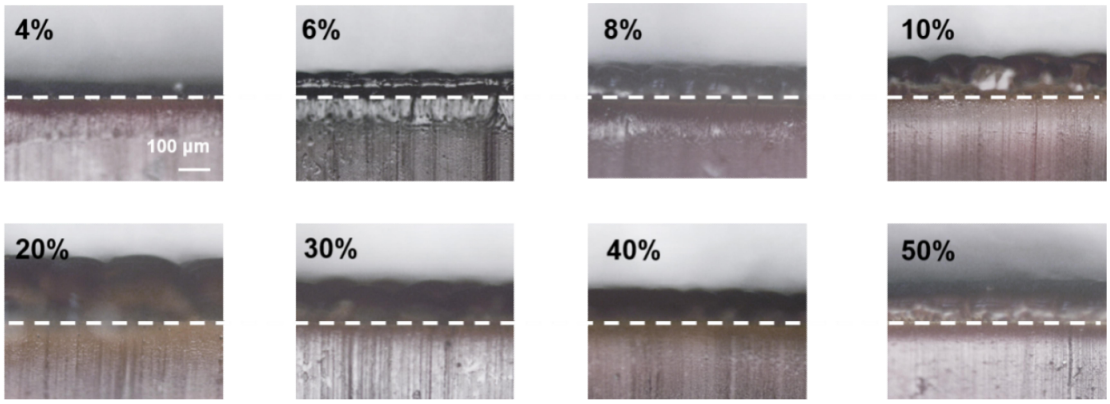


**Supplementary Fig. 10 | Concentrations-dominated thickness evolution of dissociation layer.** Cross-sectional optical microscope images for SLH samples obtained by controllable dissociation with different PAA mass concentrations (dissociation time: 8 h) to generate soft surface lubrication layer.

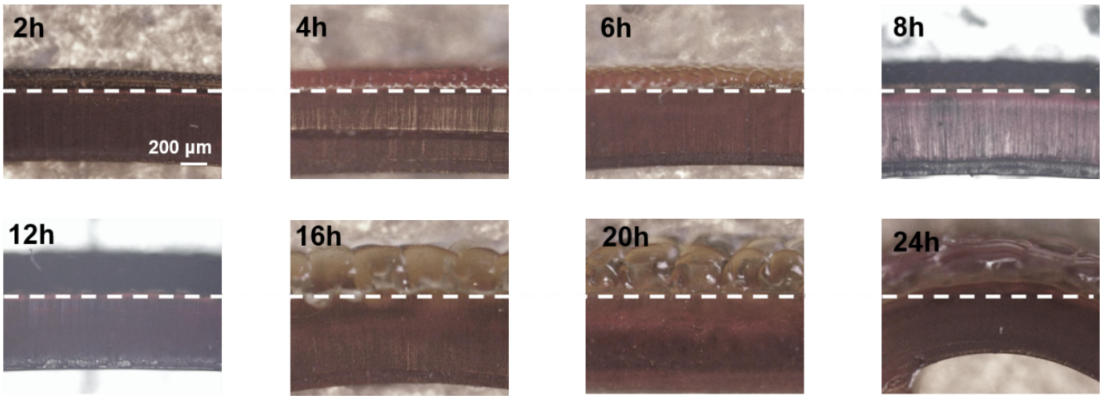


**Supplementary Fig. 11 | Time-dominated thickness evolution of dissociation layer.** Cross-sectional optical microscope images for SLH samples obtained by controllable PAA dissociation with different immersing time (mass concentration: 10%) to generate soft surface lubrication layer.

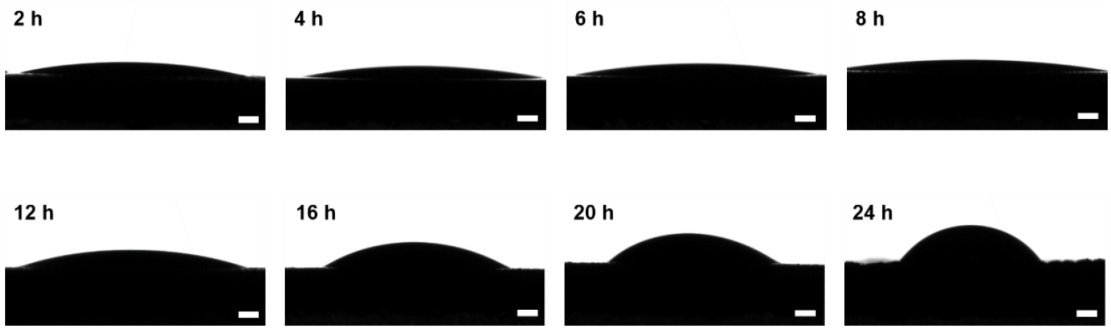


**Supplementary Fig. 12 | Time-dominated contact angle (CA) measurement.** Optical CA images of water droplet (5 μL) on the surface of SLH samples with different PAA dissociation time (mass concentration: 10%). Scale bar: 500 μm.

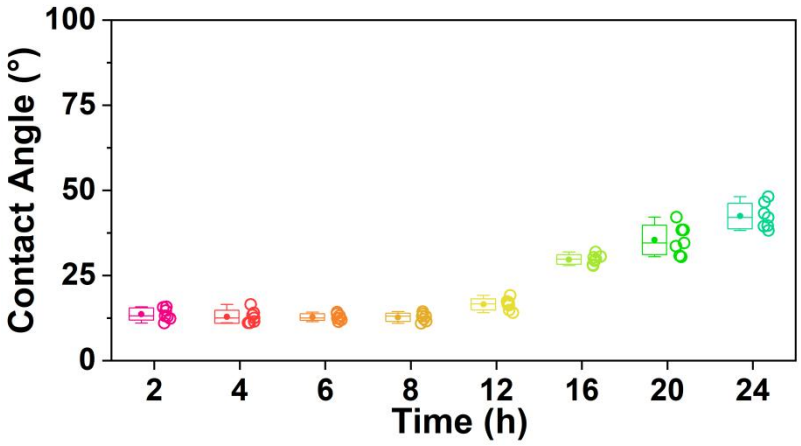


**Supplementary Fig. 13 | Time-dominated surface wettability.** Statistical results of optical contact angle (CA) values of water droplet (5 μL) on the surface of SLH samples with different PAA dissociation time (mass concentration: 10%) (n=7, the horizontal line within box represents the data value located in the middle sequence number, the upward bar represents the maximum data value and the downward bar represents the minimum data value, solid dot within box represents the average value).

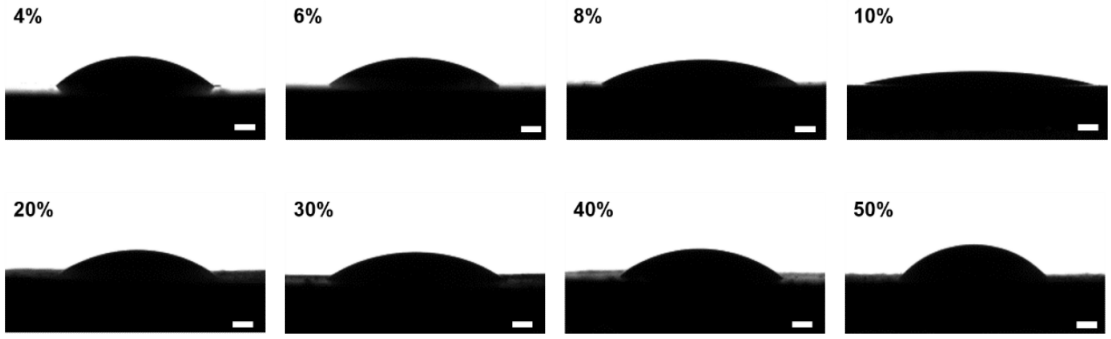


**Supplementary Fig. 14 | Concentrations-dominated contact angle (CA) measurement.** Optical CA images of water droplet (5 μL) on the surface of SLH samples obtained by controllable dissociation with different PAA mass concentrations (dissociation time: 8 h). Scale bar: 500 μm.

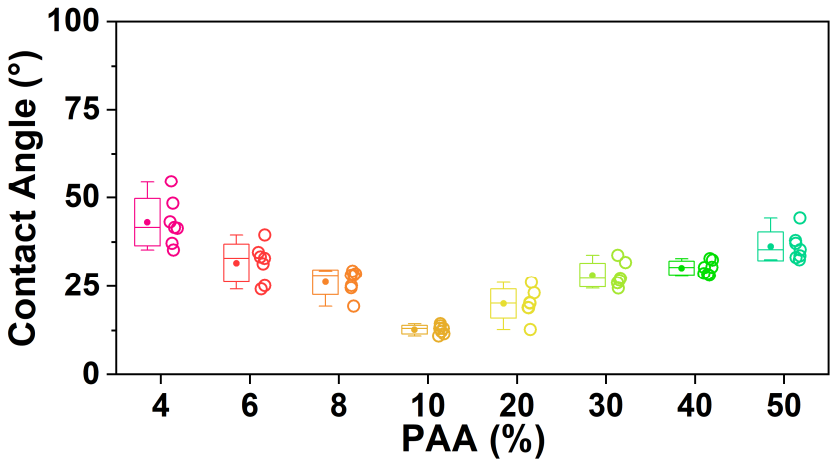


**Supplementary Fig. 15 | Concentrations-dominated surface wettability.** Statistical results of optical contact angle (CA) values of water droplet (5 μL) on the surface of SLH samples obtained by controllable dissociation with different PAA mass concentrations (dissociation time: 8 h) (n=7, the horizontal line within box represents the data value located in the middle sequence number, the upward bar represents the maximum data value and the downward bar represents the minimum data value, solid dot within box represents the average value).

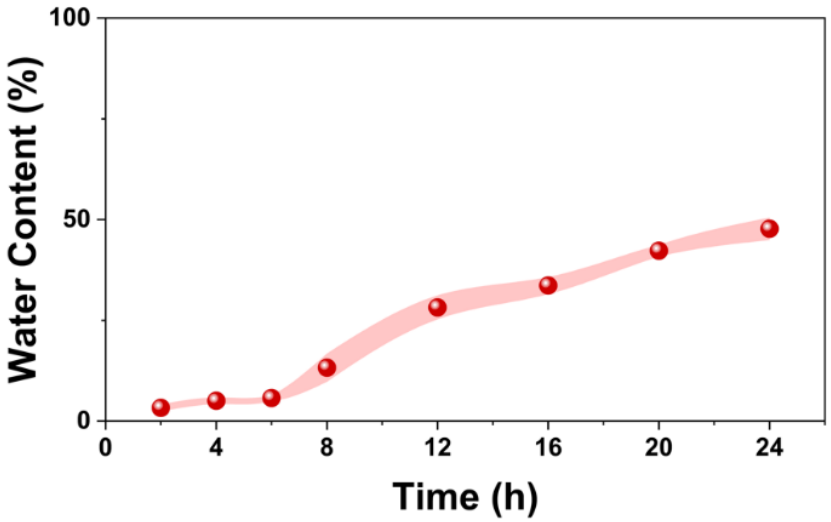


**Supplementary Fig. 16 | Time-dominated water content.** The calculated water content of dissociation lubrication layer for SLH samples obtained by controllable dissociation with different PAA immersing time (mass concentration: 10%) (n=3, mean± SD).

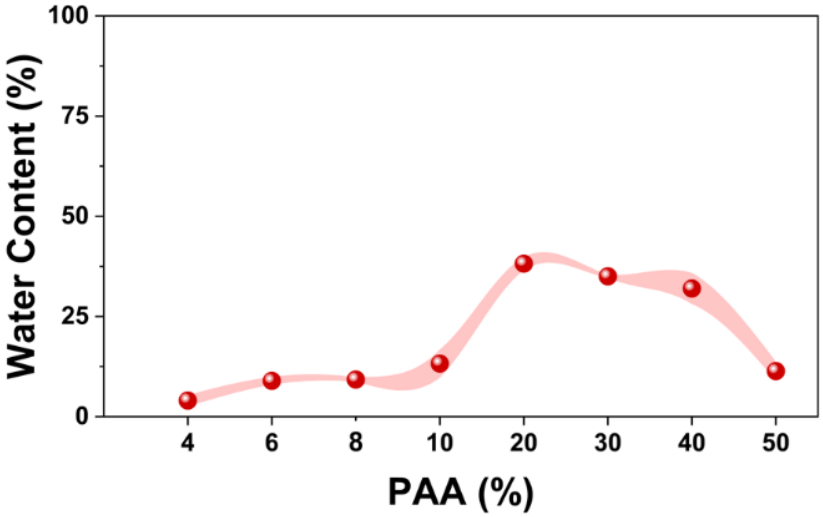


**Supplementary Fig. 17 | Concentrations-dominated water content.** The calculated water content of dissociation lubrication layer for SLH samples obtained by controllable dissociation with different PAA mass concentrations (dissociation time: 8 h) (n=3, mean± SD).

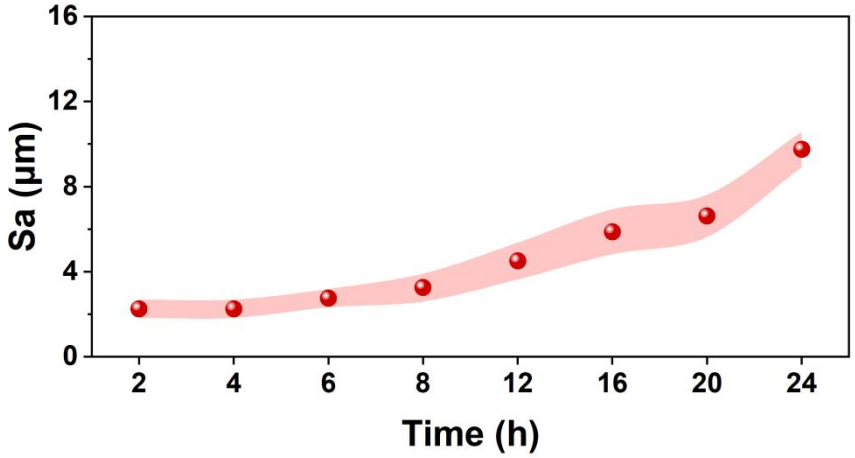


**Supplementary Fig. 18 | Time-dominated surface roughness (Sa).** The calculated Sa of dissociation lubrication layer for SLH samples obtained by controllable dissociation with different PAA immersing time (mass concentration: 10%) (n=8, mean± SD).

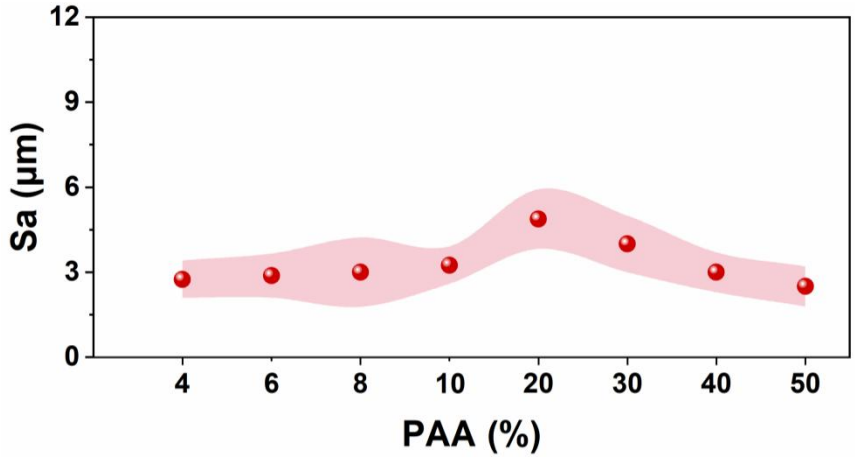


**Supplementary Fig. 19 | Concentrations-dominated surface roughness (Sa).** The calculated Sa of dissociation lubrication layer for SLH samples obtained by controllable dissociation with different PAA mass concentrations (dissociation time: 8 h) (n=8, mean± SD).

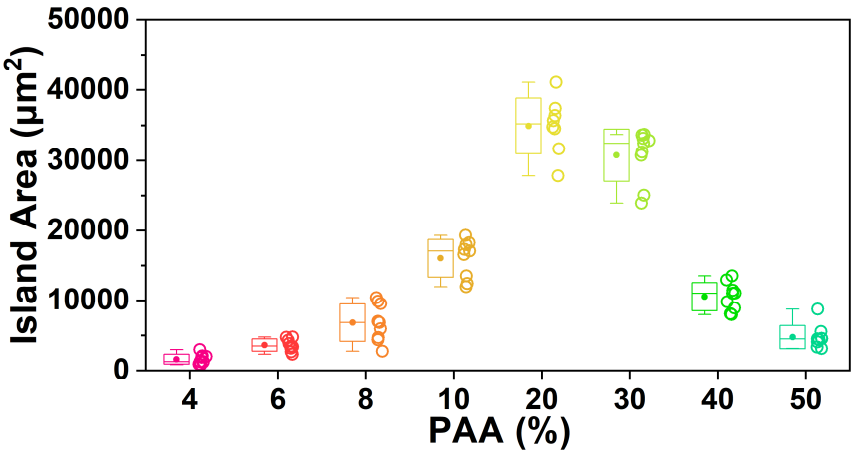


**Supplementary Fig. 20 | Concentrations-dominated island area of wrinkle.** Statistical results of single island area of wrinkle pattern on the surface of SLH samples obtained by controllable dissociation with different PAA mass concentrations (dissociation time: 8 h) (n=9, the horizontal line within box represents the data value located in the middle sequence number, the upward bar represents the maximum data value and the downward bar represents the minimum data value, solid dot within box represents the average value).

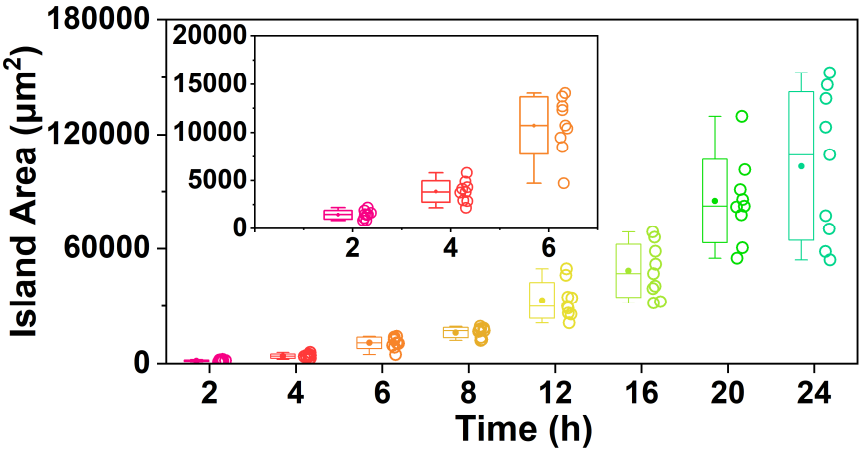


**Supplementary Fig. 21 | Time-dominated island area of wrinkle.** Statistical results of single island area of wrinkle pattern on the surface of SLH samples obtained by controllable dissociation with different PAA immersing time (mass concentrations: 10%) (n=9, the horizontal line within box represents the data value located in the middle sequence number, the upward bar represents the maximum data value and the downward bar represents the minimum data value, solid dot within box represents the average value).

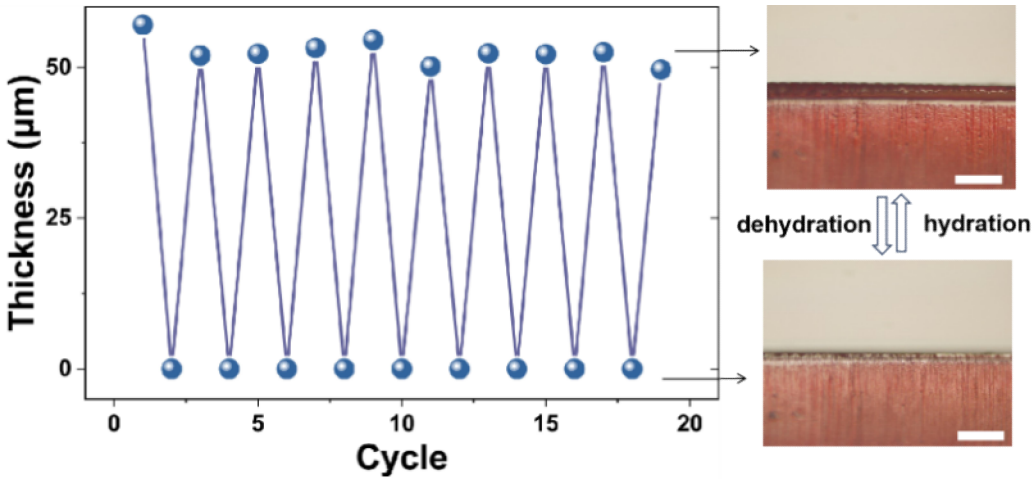


**Supplementary Fig. 22 | Reversible hydration-dehydration.** The reversible evolution of thickness for dissociation lubrication layer of SLH sample under dynamic hydration/dehydration process.

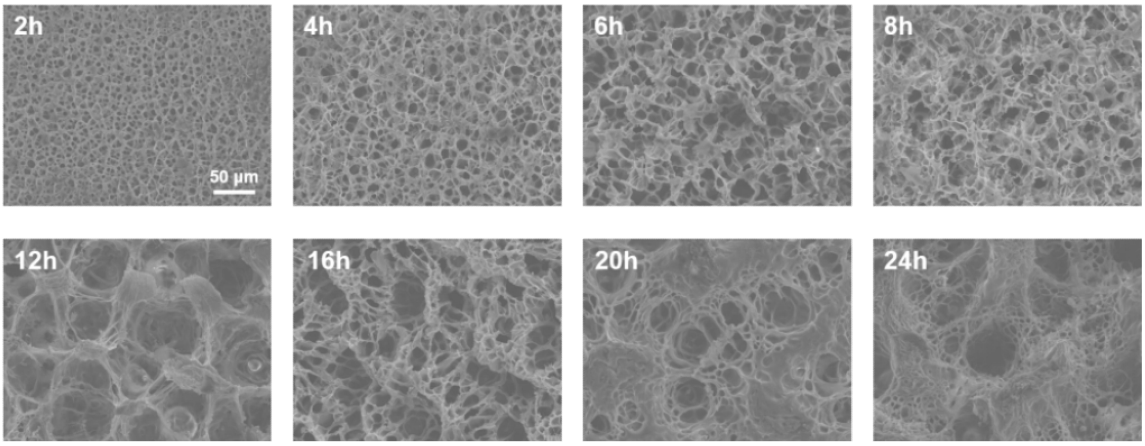


**Supplementary Fig. 23 | Time-dominated surface morphology.** Surface SEM images of the dissociation lubrication layer for SLH samples obtained by controllable dissociation with different PAA immersing time (mass concentrations: 10%).

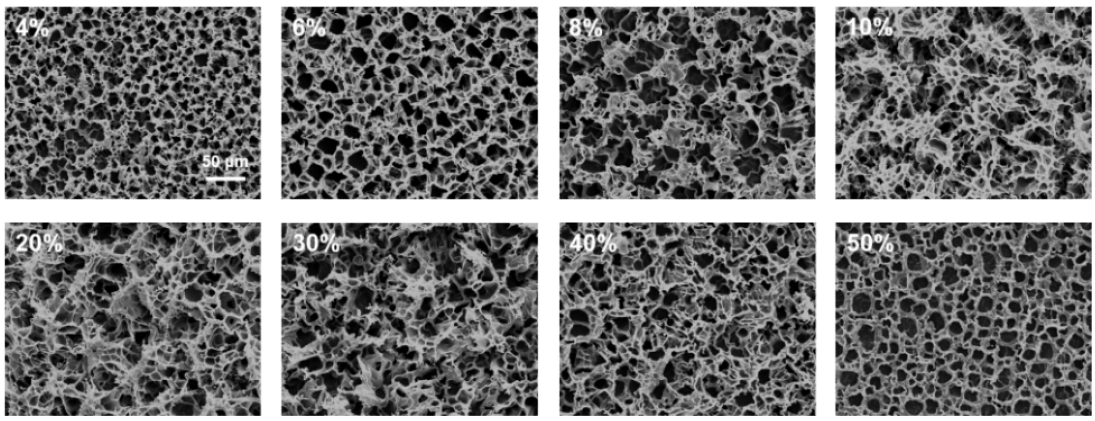


**Supplementary Fig. 24 | Concentrations-dominated surface morphology.** Surface SEM images of the dissociation lubrication layer for SLH samples obtained by controllable dissociation with different PAA mass concentrations (dissociation time: 8 h).

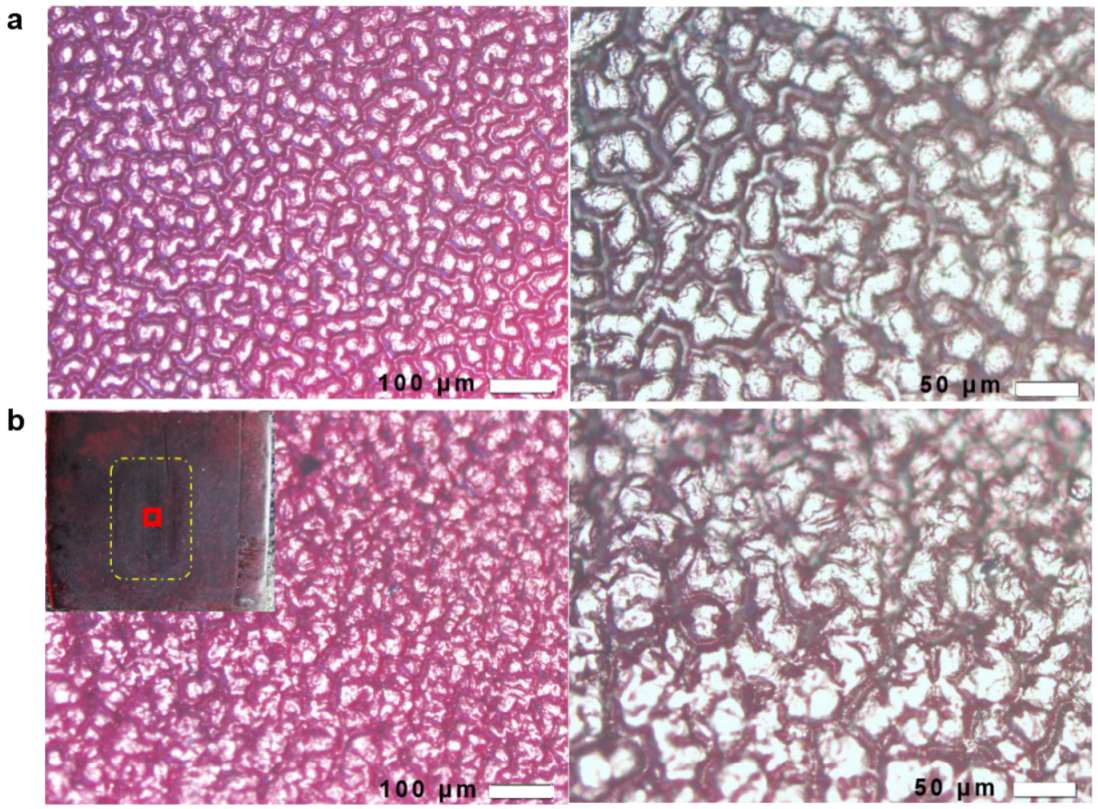


**Supplementary Fig. 25 | Surface wear characterizations.** The surface morphology of SLH sample (**a**) before friction testing and (B) after encountering 100,000 sliding cycles under constant normal load of 60 N (8.48 MPa). The photo inserted in the upper left corner of (**b**) shows the snapshot of the friction testing area (yellow dashed box), the red box represents the center position of the testing area.

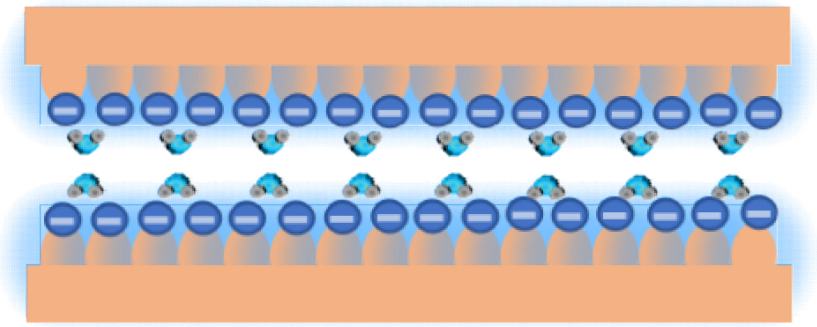

**Supplementary Fig. 26 | Lubrication mechanism for SLH.** The ultralow friction mechanism dominated by electrostatic repulsion under hydration lubrication condition.

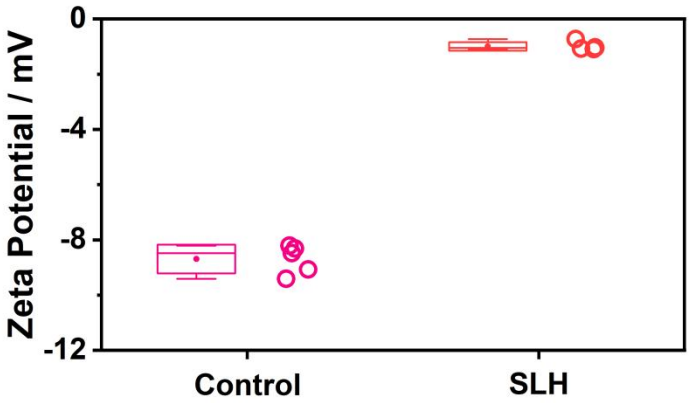


**Supplementary Fig. 27 | Surface potential measurement.** The surface Zeta potential of control sample (mechanically robust double-crosslinked hydrogel matrix) and SLH sample (n=5).

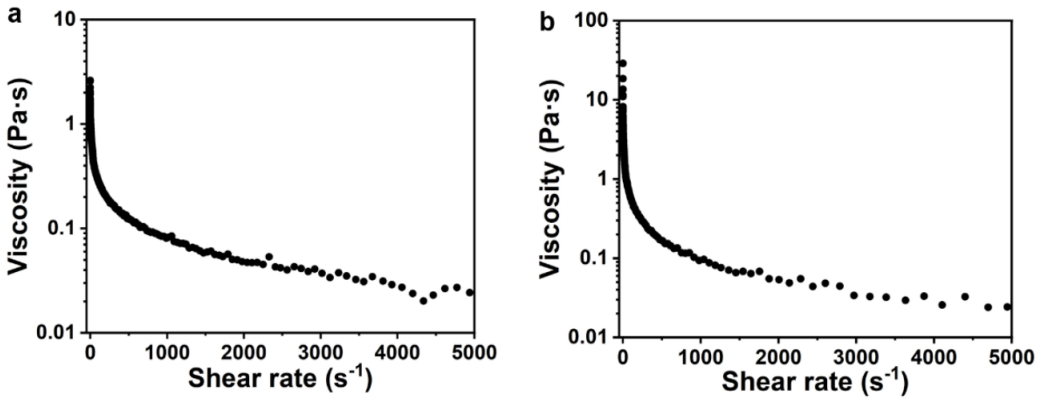


**Supplementary Fig. 28 | Viscoelasticity of lubricants.** Shear-thinning characterizations of the used commercial lubricants of (**a**) sodium alginate (SAA, 1%) and (**b**) hyaluronic acid (HA, 1%) at wide range of shearing rates (0.05 $s^{-1}$ to 5000 $s^{-1}$).

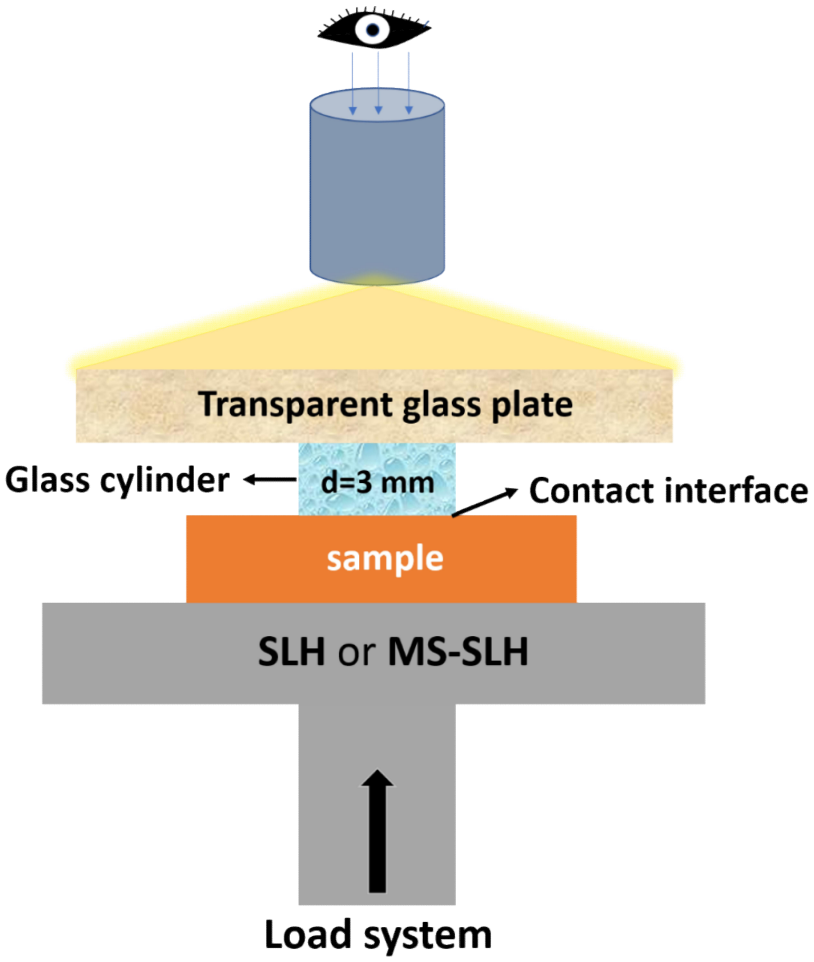


**Supplementary Fig. 29 | Self-built equipment for contact observation.** Observing the real contact state of compressed interface between MS-SLH sample and smooth glass cylinder under different normal loads condition.

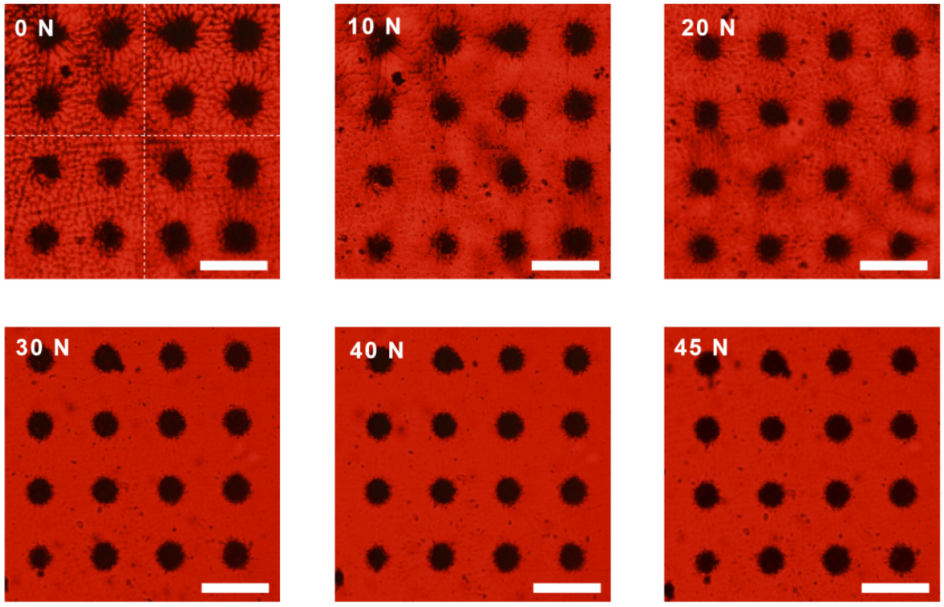


**Supplementary Fig. 30 | The evolution of contact interface at varied normal loads.** The obtained optical images for compressed contact interface of MS-SLH sample with wrinkle patterns and textured pores against smooth glass cylinder under different normal loads by a self-built observation equipment (scale bar: 200 μm, the bright red area represents the contact area, the dark black area represents the non-contact area).

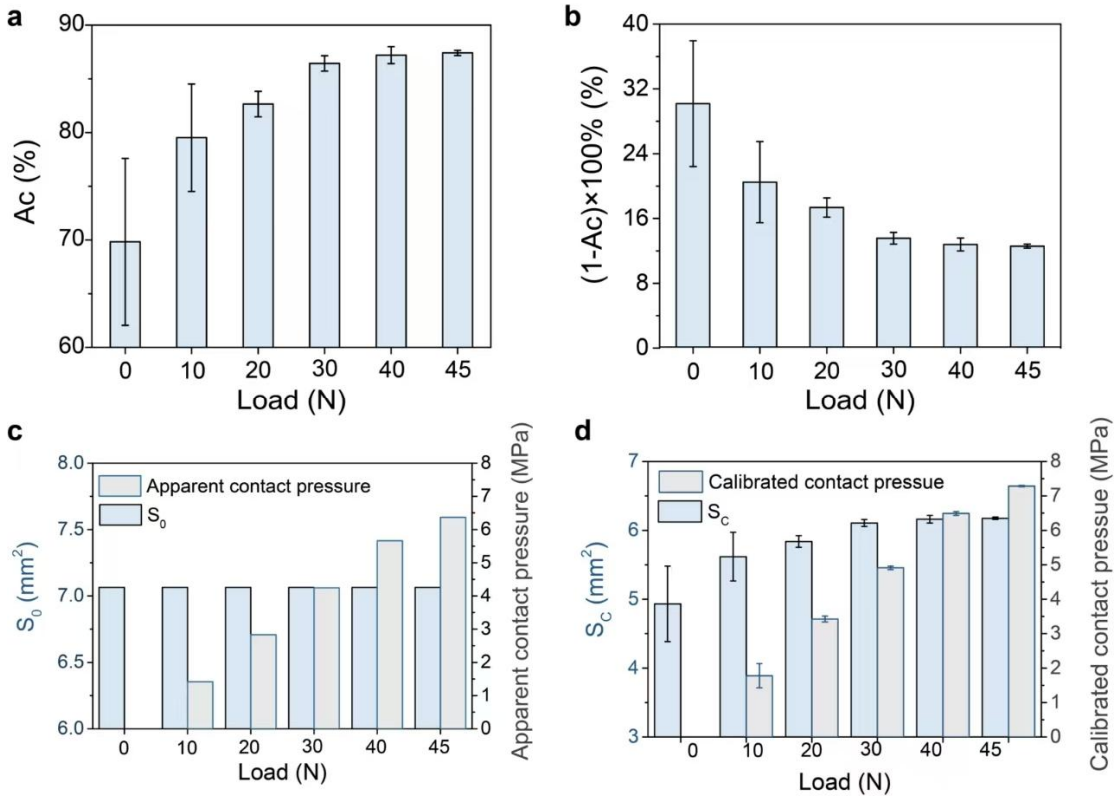


**Supplementary Fig. 31 | Measurements of contact area and contact pressure. a** The statistical change of Pixel ratio for contacted area of MS-SLH sample against smooth glass cylinder under different normal loads. **b** The change of Pixel ratio for non-contacted area of MS-SLH sample under different normal loads. **c** The calibrated average contact pressures calculated by apparent and constant contact area of $S_0$ (7.065 $mm^2$) for MS-SLH sample. **d** The calibrated average contact pressures calculated by measured contact area of $S_c$ for MS-SLH sample under different normal loads. (n=4, mean± SD)

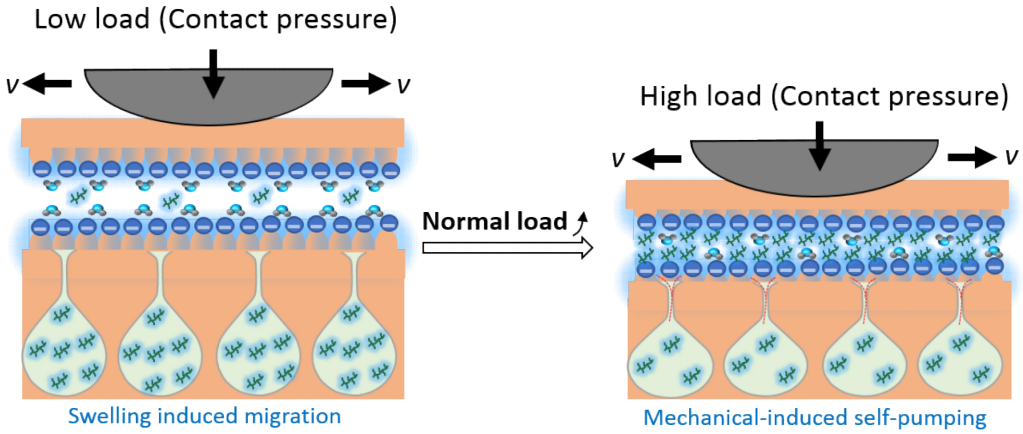


**Supplementary Fig. 32 | Lubrication mechanism for MS-SLH.** Suggested lubrication mechanism of MS-SLH sample at different normal loads (contact pressure).